HHS Public Access

Author manuscript

*Phys Med Biol*. Author manuscript; available in PMC 2017 July 07.

Published in final edited form as:

*Phys Med Biol*. 2016 July 7; 61(13): 4729–4745. doi:10.1088/0031-9155/61/13/4729.

# Simulations on the Influence of Myelin Water in Diffusion-Weighted Imaging

**Kevin D. Harkins**[1,2] and **Mark D. Does**[1,2,3,4]

[1]Department of Biomedical Engineering, Vanderbilt University

[2]Institute of Imaging Science, Vanderbilt University

[3]Department of Radiology and Radiological Sciences, Vanderbilt University

[4]Department of Electrical Engineering, Vanderbilt University

## Abstract

While myelinated axons present an important barrier to water diffusion, many models used to interpret DWI signal neglect other potential influences of myelin. In this work, Monte Carlo simulations were used to test the sensitivity of DWI results to the diffusive properties of water within myelin. Within these simulations, the apparent diffusion coefficient ($D_{app}$) varied slowly over several orders of magnitude of the coefficient of myelin water diffusion ($D_m$), but exhibited important differences compared to $D_{app}$ values simulated that neglect $D_m$ (=0). Compared to $D_{app}$, the apparent diffusion kurtosis ($K_{app}$) was generally more sensitive to $D_m$. Simulations also tested the sensitivity of $D_{app}$ and $K_{app}$ to the amount of myelin present. Unique variations in $D_{app}$ and $K_{app}$ caused by differences in the myelin volume fraction were diminished when myelin water diffusion was included. Also, expected trends in $D_{app}$ and $K_{app}$ with experimental echo time were reduced or inverted when accounting for myelin water diffusion, and these reduced/inverted trends were seen experimentally in *ex vivo* rat brain DWI experiments. In general, myelin water has the potential to subtly influence DWI results and bias models of DWI that neglect these components of white matter.

### Keywords

myelin; water; diffusion; MRI; white matter

## INTRODUCTION

Axons, and especially the myelin sheaths that surround them, present an significant barrier to water diffusion in white matter—a phenomena that has been measured with diffusion-weighted magnetic resonance imaging (DWI) to identify the structure of white matter (Basser *et al* 1994, Basser and Jones 2002) and identify white matter pathologies (Rose *et al* 2000, Horsfield *et al* 1996, Horsfield and Jones 2002). Because water density in myelin is low (Knaap and Valk 2005) and myelin water exhibits a short transverse relaxation ($T_2$)

All correspondence should be addressed to: Kevin D. Harkins, Ph.D., 1161 21st Ave South, AA-1105, Nashville, TN 37232-2310, Ph: 615-322-0219, kevin.harkins@vanderbilt.edu.

time-constant (MacKay *et al* 1994, Menon *et al* 1992, Vasilescu *et al* 1978), it is often assumed that myelin has no direct signal contribution to DWI signal. Still, it is unclear if DWI is sensitive to the amount of myelin present within white matter or to the movement of water between myelin and surrounding tissues—water in myelin may be mixing with surrounding water compartments on a time scale relevant for DWI, allowing it to contribute to the measured signal.

Analytic and computational models of DWI signal used to quantitatively assess white matter generally use one of three approximations related to myelin. First, many models considered myelin to be an impermeable boundary, restricting the extent that water can diffuse. This approximation is inherent in ActiveAx (Alexander *et al* 2010, Alexander 2008), AxCaliber (Assaf *et al* 2008), NODDI (Zhang *et al* 2012), DBSI (Wang *et al* 2011), and the WMTI model (Fieremans *et al* 2011), all of which treated the white matter DWI signal as the sum of signals from a number of non-exchanging tissue compartments—primarily intra- and extra-axonal spaces.

Second, some models include water exchange directly between intra- and extra-axonal spaces. This approach has been used both in Monte Carlo models (Ford *et al* 1998, Fieremans *et al* 2010, Nilsson *et al* 2010a), and models of coupled differential equations (Stanisz *et al* 1997, Vestergaard-Poulsen *et al* 2007). Although some work has suggested that the nodes of Ranvier provide a source of exchange (Nilsson *et al* 2010b), these approaches still neglect the potential impact of myelin as well as the potential for myelin as an intermediate region regulating water exchange between intra- and extra-axonal spaces.

Finally, a few models incorporate both the presence of myelin and water diffusion through myelin (Baxter and Frank 2013, Chin *et al* 2004, Sen and Basser 2005, Peled 2007). Within these studies, there is some debate on the coefficient of water diffusion within myelin (Sen and Basser 2005, Baxter and Frank 2013, Harkins *et al* 2012), and only one of these models consider $T_2$ differences between water compartments (Peled 2007). Further, myelin is a radially anisotropic structure, consisting of successive wrappings of lipid membrane. No model has tested the sensitivity of DWI to myelin as a radially anisotropic structure, with water able to diffuse more freely in the circumferential path (between individual lipid bilayers) and less freely in the radial direction (across lipid bilayers).

In this study, we report a series of simulations used to assess the role of myelin content and myelin water diffusion on clinical DWI. We present a new Monte Carlo model of DWI signal within myelinated axons that includes myelin sheaths as well as water diffusion within the anisotropic structure of myelin. This model is used to test the influence of these properties on the apparent diffusion coefficient ($D_{app}$) and kurtosis ($K_{app}$) measured transverse to the white matter tract orientation. These theoretical findings were then tested with a follow up DWI study in *ex vivo* rat brain.

# METHODS

## DWI Simulations in White Matter

Pulsed gradient spin echo (PGSE) experiments (Stejskal and Tanner 1965) were simulated using the Monte Carlo method. For each simulated experiment, individual sources of MR signal (i.e. "water molecules") were tracked through an arrangement of 200 myelinated axons, represented by two concentric circles. Geometries were generated as previously outlined (Hall and Alexander 2009) based upon specified values for the mean inner axon radius ($\bar{R}$), g-ratio ($g$, defined as the inner axon radius divided by outer axon radius), and intra-axonal volume fraction ($v_i$). Axon sizes were drawn from a gamma distribution ($k$=2.331, $\theta = \bar{R}/k$) (Panagiotaki *et al* 2012). An example geometry is shown in Fig 1a for $v_i$ = 0.35 and $g$ = 0.70.

## Dynamics of Water Diffusion

The biophysical properties of water in white matter were characterized by 6 parameters—the unhindered diffusion coefficient of water in intra- and extra-axonal spaces ($D_0$), the apparent diffusion coefficient of myelin water across lipid bilayers (i.e. through myelin in the radial direction, $D_{mr}$), the apparent diffusion coefficient of myelin water circumferential to the lipid bilayer surface (i.e. staying between lipid bilayers, $D_{mc}$), the transverse time-constants of water in the intra- and extra-axonal spaces ($T_{2e}$) and in myelin ($T_{2m}$), and the relative density of water in myelin compared to the intra- and extra-axonal spaces ($p_m$).

Water molecules were individually seeded through an iterative procedure to account for the difference in water density between myelin and non-myelin tissue compartments—if a potential seed was located within myelin, the location was rejected with probability 1-$p_m$ and iteratively re-seeded.

Prior to each time-step, using a combined multiple recursive algorithm (available in MATLAB as the default random number generator), two random numbers were generated for each water molecule corresponding to the random jump angle (given below as $\phi$) and the random number used to evaluate elastic reflections (given below as $P$). Within each time-step, a new random number was generated for any subsequent reflections using a linear congruential algorithm.

Within intra- and extra-axonal spaces, individual molecules jumped a fixed distance at a random angle, given by

$$\begin{aligned} \Delta x &= \sqrt{4 \cdot D_0 \cdot \Delta t} \cdot \cos(\varphi) \\ \Delta y &= \sqrt{4 \cdot D_0 \cdot \Delta t} \cdot \sin(\varphi) \end{aligned}, \quad [1]$$

where $\Delta x$, $\Delta y$ is the change in location of the molecule at each time-step, $\Delta t$ is the time-step, and $\phi$ is angular direction of the step, randomly chosen with uniform likelihood between 0 to $2\pi$. A blue circle shown in Fig 1b depicts the potential set of jumps in $\Delta x$ and $\Delta y$.

Within myelin, diffusion was considered to be radially anisotropic by breaking diffusion into circumferential and radial components

$$\begin{aligned}\Delta\theta &= \sqrt{4 \cdot D_{mc} \cdot \Delta t} \cdot \cos(\varphi)/r \\ \Delta r &= \sqrt{4 \cdot D_{mr} \cdot \Delta t} \cdot \sin(\varphi)\end{aligned}, \quad [2]$$

where $\Delta\theta$ and $\Delta r$ represent the change in angle and radius relative to the center of the axon, while $r$ is the current distance from the center of the axon. In this case, $\phi$ was drawn from a non-uniform distribution

$$p(\varphi) = \frac{r - \sqrt{4 \cdot D_{mr} \cdot \Delta t}\sin(\varphi)/2}{2\pi r}, \quad [3]$$

where $\phi = \pi/2$ points away from center of the axon. This distribution is necessary to prevent a net flux of molecules towards the center of the axon caused by breaking diffusion into circumferential and radial directions. Practically, this was implemented by taking a uniform distribution of $\phi$, then adding $\pi$ to $\phi$ with probability $P = 1 - 2 \cdot \pi \cdot p(\phi)$ (or 0 when $P$ is negative). An illustration of radially anisotropic diffusion is shown as a bent ellipse-like shape in the myelin region of Fig 1b.

For each molecule, a change in the signal phase was proportional to the applied diffusion gradient strength at each time-step

$$\Delta\phi = x_i \cdot \gamma \cdot G_{diff} \cdot \Delta t, \quad [4]$$

where $x_i$ is the location of the $i$-th molecule at the end of the present time-step, $G_{\text{diff}}$ is the applied diffusion gradient, and $\gamma$ is the gyromagnetic ratio. To incorporate $T_2$ relaxation, the signal amplitude of each water molecule ($s_n$) decayed at each time-step as $\exp[-\Delta t/T_2]$, where $T_2$ is $T_{2e}$ or $T_{2m}$ corresponding to the location of the molecule.

In intra- or extra-axonal spaces, a molecule interacting with a myelin boundary crossed into myelin with a probability

$$P = \sqrt{\frac{D_{mr}}{D_0}} \cdot p_m, \quad [5]$$

and otherwise was elastically reflected. A molecule leaving myelin experienced no boundary. Because of the change in diffusion coefficient and density of water between these compartments, this asymmetric boundary condition was required to maintain equilibrium concentrations of water molecules in each compartment (Baxter and Frank 2013).

At the experimental echo time (TE), signal was summed from the total number (N) of simulated water molecules

$$S=\frac{1}{N}\left(\sum_{n=1}^{N}s_n\cdot\cos\left(\phi_n\right)\right)/\sum_{n=1}^{N}s_n. \quad [6]$$

Simulations were implemented in CUDA, wrapped into MATLAB with the Parallel Computing Toolbox, and run on a Linux computer with a GeForce GTX TITAN GPU. For each simulated experiment, $D_{app}$ and $K_{app}$ were estimated from DWI signal using the equation (Jensen *et al* 2005)

$$\frac{S(b)}{S_0}=\exp\left[-b\cdot D_{app}+(b\cdot D_{app})^2\cdot K_{app}/6\right]. \quad [7]$$

The following parameters were held constant for all simulations: N=200,000, $\Delta t$=0.02 ms, $D_0$ = 3.0 μm$^2$/ms, $T_{2e}$ = 80 ms, $T_{2m}$ = 15 ms (MacKay *et al* 1994, Stewart *et al* 1993, Vavasour *et al* 1998), $p_m$ = 0.5 (Knaap and Valk 2005). With these parameters, an example simulation with 200 axons, $\bar{R}$ =1 μm and TE = 100 ms completes in about 100 s.

## Validation

The specific implementation of the simulation was validated to ensure that boundary conditions were being properly enforced, and that simulated signal agreed in conditions with known analytic solutions:

*Validation #1*: In the case of free diffusion (i.e. no axons), diffusion-weighted raw signals were unbiased compared to the analytic solution (i.e. $S_0$•exp[$-bD_0$]), and signal errors had an upper bound of $S_0/\sqrt{N}$.

*Validation #2*: In geometries with impermeable boundaries, molecules were not able to pass between compartments.

*Validation #3*: In geometries with impermeable boundaries, intra-axonal signal decay was in good agreement with low b-value approximated analytic solutions to diffusion within cylinders (Callaghan 1995).

*Validation #4*: In geometries with completely permeable boundaries ($p_m$ = 1, $D_0$ = $D_{mc}$ = $D_{mr}$), diffusion-weighted signal decayed with the analytic solution ($S_0$•exp[$-bD_0$]).

*Validation #5*: In geometries that included water exchange between compartments ($p_m$ = 0.5, $D_0$ = 3.0 μm$^2$/ms, $D_{mc}$ = $D_{mr}$ = $10^{-3}$ μm$^2$/ms), equilibrium concentrations of water within each compartment were stable throughout the simulation.

### Simulation Set #1: Myelin water diffusion

Simulations were performed to test the sensitivity of DWI to myelin water diffusion. A PGSE experiment was simulated ($\Delta$ = 40 ms, $\delta$ = 20 ms, and TE = 100 ms, $G_{max}$ = 0–60 mT/m in steps of 5 mT/m) in a white matter geometry with $g$ = 0.7, $v_i$ = 0.35 and $\bar{R}$ = 0.25, 1, and 4 μm. This set of parameters was selected as an example of physiologically relevant tissue. Myelin water diffusion was varied in the radial direction, $D_{mr}$ = 0, $10^{-5}$, $10^{-4}$, $10^{-3}$, $10^{-2}$, $10^{-1}$ μm$^2$/ms, while the myelin water diffusion coefficient in the circumferential direction was tested in the cases of isotropic ($D_{mc}$ = $D_{mr}$) and anisotropic myelin water diffusion ($D_{mc}$ = $D_0$). For each combination of tissue geometry, $D_{mc}$ and $D_{mr}$, the simulated signal decay at $G_{max}$ values 0, 30, and 45 mT/m (corresponding to b-values of 0, 0.85 and 1.93 ms/μm$^2$) was used to calculate $D_{app}$ and $K_{app}$. These b-values are lower than typically used for DKI (Jensen and Helpern 2010), but are suitable for simulated data without added noise.

### Simulation Set #2: Myelin content

Using the same PGSE experiment in Set #1, simulations were also performed to test if $v_m$ uniquely impacts the set of $D_{app}$ and $K_{app}$ values, or if geometries with different $v_m$ could be generated that have the same values for both $D_{app}$ and $K_{app}$. To test this hypothesis, geometries were created at two different values of $v_m$. A single geometry was generated with $v_m$ = 0.36: $v_i$ = 0.35, $g$ = 0.7, $\bar{R}$ =1 μm, and this geometry was used to compare values of $D_{app}$ and $K_{app}$ simulated with several geometries generated with $v_m$ = 0.10. Since a change in $v_m$ requires a corresponding change in the set of $v_i$ and $v_e$, geometries were generated with 6 different values in the relevant range of $v_i$ between 0.50 and 0.60. To keep $v_m$ constant, $g$ was calculated with $g = (1/(v_m/v_i+1))^{1/2}$ for each geometry. Simulations were performed with four instances of myelin water diffusion: no myelin water ($p_m$=0), water present in myelin with no myelin water diffusion ($p_m$=0.5, $D_{mr}$=$D_{mc}$=0 μm$^2$/ms), isotropic myelin water diffusion ($p_m$=0.5, $D_{mr}$=$D_{mc}$=$10^{-3}$ μm$^2$/ms), and anisotropic myelin water diffusion ($p_m$=0.5, $D_{mr}$=$10^{-3}$ μm$^2$/ms, $D_{mc}$=3.0 μm$^2$/ms).

### Simulation Set #3: Myelin Water Weighting with Short Echo times

Simulations were also used to test how $D_{app}$ and $K_{app}$ were affected by TE-dependent contributions of myelin water signal—at low values of TE, reduced decay of myelin water will increase its contribution to the measured signal. Stimulated echo diffusion experiments (Tanner 1970) ($\delta$ = 5 ms, $\Delta$ = 60 ms, mixing time = 50 ms) were used to permit TE < $\Delta$ and were run with TE = 25, 50, 75 and 100 ms. The $T_1$ relaxation time-constants of myelin and intra-/extra-axonal water were defined at 350 ms and 850 ms, respectively (Lancaster *et al* 2003). Simulations were performed in a white matter geometry with $\bar{R}$ = 1 μm, $g$ = 0.7, and $v_i$ = 0.35. Simulations were performed on same four sets of myelin water diffusion characteristics used in Simulation Set #2.

### DWI in Ex Vivo Rat Brain

This set of simulations was followed by an experimental imaging study to test the dependence of $D_{app}$ and $K_{app}$ on TE. With approval by Vanderbilt University Institutional Animal Care and Use Committee, two female Sprague Dawley rats were anesthetized with

isoflurane, perfusion fixed with 4% paraformaldehyde, and brains were dissected for *ex vivo* evaluation by MRI. Brains were imaged at bore temperature using a 15.2 T Bruker Biospec scanner (Bruker Biospin, Billerica, MA, USA). Within a 1 mm slice thickness, a field of view of 25.6 mm × 12.8 mm was encoded with 0.2 mm × 0.2 mm in-plane resolution. Stimulated echo PGSE experiments were carried out ($\delta$ = 5 ms, $\Delta$ = 60 ms, and b = 0, 4, 8, 12 & 16 μm$^2$/ms) at TE = 23, 35, 45 and 55 ms. The receiver bandwidth was set at 20 kHz, and TR was 2 s. For this data set, a single diffusion direction was collected perpendicular to the orientation of axons through the corpus callosum. Regions of interest were drawn in the cerebral cortex and the corpus callosum, and the raw signal vs b-value was fit to Eqn 7 to estimate $D_{app}$ and $K_{app}$.

## RESULTS

### Simulation Set #1

Simulations were first used to test the sensitivity of DWI to myelin water diffusion. Signal vs. b-value is shown in Fig 2 at $\bar{R}$ = 1 μm and $D_{mr}$, $D_{mc}$ = 0, $10^{-4}$, $10^{-3}$, $10^{-2}$, and $10^{-1}$ μm$^2$/ms. As $D_{mr}$ increases from 0 to $10^{-3}$ μm$^2$/ms the overall rate of signal decay with b-value decreases. This is due an increased amount of signal from water that has resided in the slowly diffusing myelin water compartment at some point during the diffusion weighting, reflecting that while water is still greatly restricted, it has become sufficiently mobile that it can enter and leave myelin before its signal is lost by transverse relaxation. As $D_{mr}$ increases further, the effect on signal decay reverses, meaning that myelin has become less restrictive to water diffusion. In the case of $D_{mr} = 10^{-1}$ μm$^2$/ms, myelin provide little barrier to diffusion resulting in a near mono-exponential signal decay with b-value.

$D_{app}$ and $K_{app}$ from this set of simulations are given in Fig 3. In general, an increase in $\bar{R}$ causes an increase in $D_{app}$, and a decrease in $K_{app}$. $D_{app}$ varies slowly over several orders of magnitude in $D_{mr}$. However as $D_{mr}$ increases from 0, there is an initial slight decrease in $D_{app}$ present in most curves, followed by an increase. In cases of anisotropic myelin water diffusion (dashed lines), $D_{app}$ deviates from its isotropic values (solid lines) primarily where $D_{mr} \geq 10^{-3}$ μm$^2$/ms.

Overall, $K_{app}$ is more sensitive to myelin water diffusion. $K_{app}$ is decreased in regions where water can easily diffuse through myelin. Plots show an intermediate increase in $K_{app}$ with an increase in $D_{mr}$, caused by an increase in the apparent contribution of water from the slow-diffusing myelin compartment. Throughout this range in $D_{mr}$, $K_{app}$ within tissues with anisotropic myelin water diffusion did not greatly differ from the values simulation within geometries with isotropic myelin water diffusion.

### Simulation Set #2

A second set of simulations were performed to test if myelin content can uniquely inform basic DWI measurements. To illustrate the effect of myelin content, relative differences in $D_{app}$ and $K_{app}$ calculated as

$$\Delta D_{app} = \frac{D_{app}\,(v_m{=}0.1) - D_{app}\,(v_m{=}0.36, v_i{=}0.35)}{D_{app}\,(v_m{=}0.36, v_i{=}0.35)} \cdot 100\% \quad [8]$$

$$\Delta K_{app} = \frac{K_{app}\,(v_m{=}0.1) - K_{app}\,(v_m{=}0.36, v_i{=}0.35)}{K_{app}\,(v_m{=}0.36, v_i{=}0.35)} \cdot 100\% \quad [9]$$

are plotted in Fig 4. Since this change in $v_m$ also requires a change in $v_i$ and/or $v_e$, $\Delta D_{app}$ and $\Delta K_{app}$ are plotted vs. $v_i$, representing the range in $v_i$ (and $v_e$) that provide similar values for $D_{app}$ and $K_{app}$. Solid lines connect $\Delta D_{app}$ (blue) and $\Delta K_{app}$ (red) in the case of no water diffusion, while dashed lines represent simulated values with isotropic myelin water diffusion. Values of $\Delta D_{app}$ and $\Delta K_{app}$ from simulations with no myelin water and anistropic myelin water diffusion are not shown, as those curves depict similar characteristics to those with no myelin water diffusion and isotropic myelin water diffusion, respectively. As predicted in other models, a simple increase in $v_i$ caused a decrease in $D_{app}$ and an increase in $K_{app}$ due to an increase in the fraction of restricted intra-axonal water (Szafer *et al* 1995, Fieremans *et al* 2011).

When myelin water diffusion was neglected, these simulations indicate that a difference in $v_m$ caused a change in the values of either $D_{app}$ or $K_{app}$ or changed both values depending on the selected value of $v_i$. It was impossible to generate a geometry with $v_m = 0.1$ where both $D_{app}$ and $K_{app}$ values were unchanged relative to a geometry with $v_m = 0.36$. For example, the relative value of $K_{app}$ was unchanged at $v_i \approx 0.515$m, but $D_{app}$ was increased by ≈10–15%. While this seems to imply that a set of $D_{app}$ and $K_{app}$ values could be used determine myelin content, the introduction of myelin water diffusion reduced the differences in these values—when $D_{mr} = 10^{-3}$ μm$^2$/ms, $\Delta D_{app}$ and $\Delta K_{app}$ are unchanged (=0) at $v_i \approx 0.57$.

### Simulation Set #3

A third set of simulations were performed to test how modeling of myelin water and myelin water diffusion affected the TE dependent nature of $D_{app}$ and $K_{app}$, as shown in Fig 5. In theory, shorter echo times could be used to increase the contribution of the slowly diffusing myelin water to measured DWI signal. This was obviously not seen in the simulations that included no myelin water. $D_{app}$ decreased and $K_{app}$ increased at lower values of TE when myelin water was included, with $D_{mr} = 0$. However, when myelin water diffusion was included in the simulation, this trend was reversed.

### DWI in Ex Vivo Rat Brain

An example *ex vivo* rat brain image is given in Fig 6, along with corresponding plots showing the dependence of $D_{app}$ and $K_{app}$ on TE in two rat brains (represented as solid and dashed lines) within regions of interest in the cerebral cortex and corpus callosum. For both rats imaged, $D_{app}$ in the corpus callosum was largely independent of TE, while $K_{app}$ increased in the same range. In cerebral cortex, $D_{app}$ decreased and $K_{app}$ increased with TE.

# DISCUSSION

While myelin serves as an important source of restriction measured by DWI, this study indicates that myelin water diffusion has the potential to make subtle but important influences on DWI measurements.

## Myelin Water Diffusion

Recent interest in the role of myelin water diffusion on DWI signal has been motivated in part by multi-component $T_2$ relaxation studies investigating signal from myelin water. While the myelin water fraction ($f_{my}$) has been used as an estimate of myelin content (MacKay *et al* 1994, Menon *et al* 1992, Vasilescu *et al* 1978, Laule *et al* 2002), recent studies have suggested that $f_{my}$ underestimates myelin content in regions with thin myelin (Dula *et al* 2010). To explain the discrepancy between $f_{my}$ and histologic myelin volume fraction, a computational model estimated a myelin water diffusion coefficient of $D_{mr} \approx 10^{-3}$ μm$^2$/ms (Harkins *et al* 2012). While this value of $D_{mr}$ generally agrees with measurements of water diffusion through synthetic myelin (Khakimova *et al* 2008), a couple studies have indirectly estimated that water exchange through myelin is much slower than this value would suggest (Laule *et al* 2004, Kalantari *et al* 2011). Within the context of these previous studies, the physiologic value of $D_{mr}$ is estimated to be between 0 and $10^{-3}$ μm$^2$/ms.

Within these bounds, our data suggest that myelin water diffusion has the potential to influence DWI experiments and bias analysis that does not take into account water movement between compartments. While $D_{app}$ varied slowly over several orders of magnitude of $D_{mr}$, there were important differences compared to its value in the no-diffusion limit ($D_{mr} \rightarrow 0$). Specifically, $D_{app}$ values decreased as $D_{mr}$ increased from 0. While this trend may be somewhat counterintuitive, the decrease in $D_{app}$ with an increase in $D_{mr}$ is caused by an increased contribution of signal from the slow diffusing (and short $T_2$) myelin compartment, aided by movement of water between compartments. Relative to $D_{app}$, $K_{app}$ was somewhat more sensitivity to the rate of myelin water diffusion. Similar to the bimodal nature of $D_{app}$, $K_{app}$ initially increased with an increase in $D_{mr}$, caused by an increased contribution from slowly-diffusion myelin water.

While the present study neglects the potential for exchange directly between intra- and extra-axonal compartments, some work has suggested that exchange can happen directly between these compartments at Nodes of Ranvier (Nilsson *et al* 2010b). While it is unclear how direct exchange of water between these compartments would impact the current results, the bi-modal features of Fig 3 with $D_{mr}$ will be absent from models that ignore $T_2$ variations between myelin and non-myelin components of tissue (Harkins *et al* 2009).

## Anisotropic Myelin Water Diffusion

Anisotropic diffusion within myelin is supported both by the structure of myelin mentioned earlier and diffusion experiments that have estimated diffusion in myelin. Experiments in synthetic myelin have measured very slow diffusion orthogonal to the lipid bilayer surface (represented as $D_{mr}$ in the present work) and faster diffusion along the lipid bilayer surface (i.e. $D_{mc}$) (Khakimov *et al* 2008). In other experiments, combined multi-exponential $T_2$ and

diffusion experiments have been used to measure $D_{app}$ of the myelin water $T_2$ component, which was estimated to be > 0.1 $\mu m^2/ms$ (Andrews *et al* 2006, Stanisz and Henkelman 1998). This value represents a mixture of $D_{mr}$ and $D_{mc}$, as water is able to diffuse around axons as well as through myelin within those experiments. Further, those estimates of myelin water diffusion may be sensitive to any movement of water between compartments.

As part of this work, we tested the sensitivity of DWI measurements to the anisotropic structure of myelin. While $D_{app}$ was higher in some geometries containing anisotropic myelin water diffusion, this was primarily at the edge of what is considered the physiologic range in $D_{mr}$.

### Sensitivity of DWI to Myelin Content

Another question posed by this work is whether the amount of myelin present in tissue can affect DWI signal in a unique way, or if it is possible to generate geometries with different amounts of myelin that produce effectively identical $D_{app}$ and $K_{app}$. Previous work has hypothesized that myelin content could affect $D_{app}$ and $K_{app}$ (Fieremans *et al* 2011), while even a simple analytic model of DWI generally supports the role of myelin content to uniquely influence DWI measurements. Consider a three-compartment model with intra- (i.e. slowly diffusing) and extra-axonal (i.e. faster diffusing) compartments, where myelin (the third compartment) does not contribute to the measured signal. The extra-axonal signal fraction ($f_e$) would be characterized by

$$f_e=\frac{v_e}{v_i+v_e}=\frac{v_e}{1-v_m}. \quad [10]$$

Meanwhile the rate of extra-axonal diffusion ($D_e$) is primarily a function of $v_e$. In the long diffusion-time limit,

$$D_e=v_e D_0 \quad [11]$$

(Latour *et al* 1994, Lam *et al* 2014). In theory, these two measures could be used to quantify myelin content,

$$v_m=1-\frac{D_e}{D_0 f_e}. \quad [11]$$

Since the simulations contained in the present work are not in the long diffusion-time limit for extracellular space, Eqn [11] represents a simplified model of extra-axonal water diffusion. It is beyond the scope of this work to fully characterize $D_e/D_0$ in terms of $v_e$ and the cellular spacing relative to the probed diffusion time. However in the case that myelin water diffusion can be neglected, the present simulation study implies that this type of

estimation for myelin content is possible—in the solid lines of Fig 4 where myelin water diffusion is neglected, there is no value of $v_i$ over which both $\Delta D_{app}$ and $\Delta K_{app}$ are negated.

Still, these simulations suggest that myelin water exchange further complicates these relationships—the influence of myelin content on DWI is reduced when myelin water diffusion is included. Within the dashed lines in Fig 4, which includes myelin water diffusion, $\Delta D_{app}$ and $\Delta K_{app}$ both cross zero near $v_i \approx 0.57$.

## Myelin Water Weighting

Similar to its effect on myelin content dependent diffusion changes, myelin water diffusion also changes the influence of TE on $D_{app}$ and $K_{app}$. In the present work, when excluding myelin water diffusion, $D_{app}$ increases and $K_{app}$ decreases with increasing TE, indicating a decreased weighting of myelin water within the acquired signal. To our knowledge, there are no studies of DWI in white matter that report such an increase in $D_{app}$ with echo time. One previous study in white matter found no difference between spin-echo and stimulated-echo DWI measurements at different echo times (Avram *et al* 2010), while another study in white matter showed a decrease in the radial diffusion eigenvalues with echo time at 1.5 and 3T (Qin *et al* 2009). A slight trend in $D_{app}$ with TE was observed in ex vivo rat corpus callosum in the present work, shown in Fig 6.

While this generally agrees with trends in $D_{app}$ and $K_{app}$ under the influence of myelin water diffusion predicted by simulation in Fig 5, a decrease in $D_{app}$ and/or an increase in $K_{app}$ with TE could also occur if the restricted intra-axonal space had a longer intrinsic $T_2$ relaxation time-constant than extra-axonal space. There is direct evidence for such an assignment of intra- and extra-axonal $T_2$ components in peripheral nerve (Peled *et al* 1999, Wachowicz and Snyder 2002, Dortch *et al* 2010, Does and Gore 2000), which is known to contain three $T_2$ components (Vasilescu *et al* 1978). For instance, in frog sciatic nerve it has been shown that a long $T_2$ component (≈300 ms) exhibited a generally lower rate of water diffusion than the intermediate $T_2$ component (Peled *et al* 1999). In contrast to peripheral nerve, only two $T_2$ components are generally observed in white matter (Menon *et al* 1992, MacKay *et al* 1994); however, a couple studies have suggested that distinct intra- and extra-axonal $T_2$ components were required to explain findings on myelin water exchange in spinal cord and optic nerve (Dortch *et al* 2013, Harkins *et al* 2012). Thus, the trends in $D_{app}$ and $K_{app}$ observed in Fig 6 with echo time could indicate either myelin water diffusion or $T_2$ differences between intra- and extra-axonal compartments. Future work is aimed at investigating the influence of distinct intra- and extra-axonal $T_2$ relaxation time-constants in DWI and the potential to experimentally separate these influences to evaluate the influence of myelin water diffusion directly.

It should be noted that the decrease in $D_{app}$ with TE measured in cerebral cortex is in disagreement with several previous studies that investigated echo time dependent effects in gray matter (Does and Gore 2000, Vestergaard-Poulsen *et al* 2007, Buckley and Blackband 1999), and may reflect changes in tissue associated with fixation.

### Limitations of the Present Study

There are several methodological limitations to the current work. Previous work has suggested that intra- and extra-axonal $T_2$ may not be equivalent (Harkins *et al* 2009, 2012, Vestergaard-Poulsen *et al* 2007). Further, within this work, $D_0$ is taken as the diffusion of free water at body temperature; however, the value of $D_0$ in tissue may be reduced by macromolecular components in intra- and extra-axonal compartments, and may even differ between these compartments. Also within this work, $g$ is independent of $R$, which is not generally true (Berthold *et al* 1983, Chatzopoulou *et al* 2008, Crawford *et al* 2010). The shape of the distribution of axon sizes may not be constant with mean axon size, and may even be log-linear instead of gamma distributed (Buzsaki and Mizuseki 2014). Still, this work contains the most microstructrually complex model of axons published so far, as it considers the structure of myelin sheaths.

## CONCLUSIONS

$D_{app}$ and $K_{app}$ measured by DWI represent a complicated set of interactions between water and its local environment that are not completely understood. The results presented in this manuscript indicate that myelin water could present subtle but important contributions to DWI results. For instance, $D_{app}$ and $K_{app}$ simulated with physiologic values of myelin water diffusion were biased by up to and around 10% compared to simulations that neglected myelin water. It is also shown that myelin water diffusion can change the TE-dependence of $D_{app}$ and $K_{app}$, although other mechanisms could also cause TE-dependent variations in $D_{app}$ and $K_{app}$ observed in white matter. Given the limited sensitivity of the simulated data to the diffusion characteristics of myelin water, it remains unclear whether the reported trends will be useful in clinical imaging. Still, as complex models of DWI signal are increasingly applied to experimental and clinical MRI, it is important to understand the full range of biophysical properties that could affect DWI results.

## Acknowledgments

**Grant sponsors:** NIH R01 EB001744

## References

Alexander DC. A general framework for experiment design in diffusion MRI and its application in measuring direct tissue-microstructure features. Magn Reson Med. 2008; 60:439–48. [PubMed: 18666109]

Alexander DC, Hubbard PL, Hall MG, Moore Ea, Ptito M, Parker GJM, Dyrby TB. Orientationally invariant indices of axon diameter and density from diffusion MRI. Neuroimage. 2010; 52:1374–89. [PubMed: 20580932]

Andrews TJ, Osborne MT, Does MD. Diffusion of myelin water. Magn Reson Med. 2006; 56:381–5. [PubMed: 16767712]

Assaf Y, Blumenfeld-Katzir T, Yovel Y, Basser PJ. AxCaliber: a method for measuring axon diameter distribution from diffusion MRI. Magn Reson Med. 2008; 59:1347–54. [PubMed: 18506799]

Avram AV, Guidon A, Song AW. Myelin water weighted diffusion tensor imaging. Neuroimage. 2010; 53:132–8. [PubMed: 20587369]

Basser PJ, Jones DK. Diffusion-tensor MRI: theory, experimental design and data analysis - a technical review. NMR Biomed. 2002; 15:456–67. [PubMed: 12489095]

Basser P, Mattiello J, LeBihan D. MR diffusion tensor spectroscopy and imaging. Biophys J. 1994; 66:259–67. [PubMed: 8130344]

Baxter GT, Frank LR. A computational model for diffusion weighted imaging of myelinated white matter. Neuroimage. 2013; 75:204–12. [PubMed: 23507381]

Berthold C, Nilsson I, Rydmark M. Axon diameter and myelin sheath thickness in nerve fibres of the ventral spinal root of the seventh lumbar nerve of the adult and developing cat. J Anat. 1983; 136:483–508. [PubMed: 6885614]

Buckley DL, Blackband SJ. The effect of ouabain on water diffusion in the rat hippocampal slice measured by high resolution NMR imaging. Magn Reson Med. 1999; 41:137–42. [PubMed: 10025621]

Buzsaki G, Mizuseki K. The log-dynamic brain: how skewed distributions affect network operations. Nat Rev Neurosci. 2014; 15:264–78. [PubMed: 24569488]

Callaghan PT. Pulsed-Gradient spin-echo NMR for Planar, Cylindrical, and Spherical Pores under Conditions of Wall Relaxation. J Magn Reson Ser A. 1995; 113:53–9.

Chatzopoulou E, Miguez A, Savvaki M, Levasseur G, Muzerelle A, Muriel M-P, Goureau O, Watanabe K, Goutebroze L, Gaspar P, Zalc B, Karagogeos D, Thomas J-L. Structural requirement of TAG-1 for retinal ganglion cell axons and myelin in the mouse optic nerve. J Neurosci. 2008; 28:7624–36. [PubMed: 18650339]

Chin C-L, Wehrli FW, Fan Y, Hwang SN, Schwartz ED, Nissanov J, Hackney DB. Assessment of axonal fiber tract architecture in excised rat spinal cord by localized NMR q-space imaging: simulations and experimental studies. Magn Reson Med. 2004; 52:733–40. [PubMed: 15389948]

Crawford DK, Mangiardi M, Song B, Patel R, Du S, Sofroniew MV, Voskuhl RR, Tiwari-Woodruff SK. Oestrogen receptor beta ligand: a novel treatment to enhance endogenous functional remyelination. Brain. 2010; 133:2999–3016. [PubMed: 20858739]

Does MD, Gore JC. Compartmental study of diffusion and relaxation measured in vivo in normal and ischemic rat brain and trigeminal nerve. Magn Reson Med. 2000; 43:837–44. [PubMed: 10861878]

Dortch RD, Harkins KD, Juttukonda MR, Gore JC, Does MD. Characterizing inter-compartmental water exchange in myelinated tissue using relaxation exchange spectroscopy. Magn Reson Med. 2013:1450–9. [PubMed: 23233414]

Dortch RD, Apker GA, Valentine WM, Lai B, Does MD. Compartment-specific enhancement of white matter and nerve ex vivo using chromium. Magn Reson Med. 2010; 64:688–97. [PubMed: 20806376]

Dula AN, Gochberg DF, Valentine HL, Valentine WM, Does MD. Multiexponential T2, magnetization transfer, and quantitative histology in white matter tracts of rat spinal cord. Magn Reson Med. 2010; 63:902–9. [PubMed: 20373391]

Fieremans E, Jensen JH, Helpern Ja. White matter characterization with diffusional kurtosis imaging. Neuroimage. 2011; 58:177–88. [PubMed: 21699989]

Fieremans E, Novikov DS, Jensen JH, Helpern Ja. Monte Carlo study of a two-compartment exchange model of diffusion. NMR Biomed. 2010; 23:711–24. [PubMed: 20882537]

Ford JC, Hackney DB, Lavi E, Phillips M, Patel U. Dependence of apparent diffusion coefficients on axonal spacing, membrane permeability, and diffusion time in spinal cord white matter. J Magn Reson Imaging. 1998; 8:775–82. [PubMed: 9702877]

Hall MG, Alexander DC. Convergence and parameter choice for Monte-Carlo simulations of diffusion MRI. IEEE Trans Med Imaging. 2009; 28:1354–64. [PubMed: 19273001]

Harkins KD, Dula AN, Does MD. Effect of intercompartmental water exchange on the apparent myelin water fraction in multiexponential T2 measurements of rat spinal cord. Magn Reson Med. 2012; 67:793–800. [PubMed: 21713984]

Harkins KD, Galons J-P, Secomb TW, Trouard TP. Assessment of the effects of cellular tissue properties on ADC measurements by numerical simulation of water diffusion. Magn Reson Med. 2009; 62:1414–22. [PubMed: 19785014]

Horsfield, Ma; Lai, M.; Webb, SL.; Barker, GJ.; Tofts, PS.; Turner, R.; Rudge, P.; Miller, DH. Apparent diffusion coefficients in benign and secondary progressive multiple sclerosis by nuclear magnetic resonance. Magn Reson Med. 1996; 36:393–400. [PubMed: 8875409]

Horsfield, Ma; Jones, DK. Applications of diffusion-weighted and diffusion tensor MRI to white matter diseases - A review. NMR Biomed. 2002; 15:570–7. [PubMed: 12489103]

Jensen JH, Helpern Ja, Ramani A, Lu H, Kaczynski K. Diffusional kurtosis imaging: the quantification of non-gaussian water diffusion by means of magnetic resonance imaging. Magn Reson Med. 2005; 53:1432–40. [PubMed: 15906300]

Jensen JH, Helpern Ja. MRI quantification of non-Gaussian water diffusion by kurtosis analysis. NMR Biomed. 2010; 23:698–710. [PubMed: 20632416]

Kalantari S, Laule C, Bjarnason TA, Vavasour IM, MacKay AL. Insight into in vivo magnetization exchange in human white matter regions. Magn Reson Med. 2011; 66:1142–51. [PubMed: 21381107]

Khakimov, aM; Rudakova, Ma; Doroginitskii, MM.; Filippov, aV. Temperature dependence of water self-diffusion through lipid bilayers assessed by NMR. Biophysics (Oxf). 2008; 53:147–52.

Khakimova AM, Rudakova MA, Doroginitskii MM, Filippov AV. An NMR study of the temperature dependence of the coefficient of water self-diffusion through lipid bilayer membranes. Biofizika. 2008; 53:271–80. [PubMed: 18543769]

van der Knaap, MS.; Valk, J. Magnetic Resonance of Myelination and Myelin Disorders. Berlin, New York: Springer; 2005. p. 7

Lam WW, Jbabdi S, Miller KL. A model for extra-axonal diffusion spectra with frequency-dependent restriction. Magn Reson Med. 2014; 73:2306–20. [PubMed: 25046481]

Lancaster JL, Andrews T, Hardies LJ, Dodd S, Fox PT. Three-pool model of white matter. J Magn Reson Imaging. 2003; 17:1–10. [PubMed: 12500269]

Latour LL, Svoboda K, Mitra PP, Sotak CH. Time-dependent diffusion of water in a biological model system. Proc Natl Acad Sci U S A. 1994; 91:1229–33. [PubMed: 8108392]

Laule C, Vavasour IM, Moore GRW, Oger J, Li DKB, Paty DW, MacKay aL. Water content and myelin water fraction in multiple sclerosis A T2 relaxation study. J Neurol. 2004; 251:284–93. [PubMed: 15015007]

Laule, C.; Vavasour, IM.; Paty, D.; Li, D.; Arnold, DL.; MacKay, A. Correlation between magnetization transfer and myelin water content in normal white matter and MS lesions. Proc ISMRM; Honolulu, HI. 2002. p. 182

MacKay A, Whittall K, Adler J, Li D, Paty D, Graeb D. In vivo visualization of myelin water in brain by magnetic resonance. Magn Reson Med. 1994; 31:673–7. [PubMed: 8057820]

Menon RS, Rusinko MS, Allen PS. Proton relaxation studies of water compartmentalization in a model neurological system. Magn Reson Med. 1992; 28:264–74. [PubMed: 1281258]

Nilsson M, Alerstam E, Wirestam R, Stahlberg F, Brockstedt S, Latt J. Evaluating the accuracy and precision of a two-compartment Karger model using Monte Carlo simulations. J Magn Reson. 2010a; 206:59–67. [PubMed: 20594881]

Nilsson M, Hagslatt H, van Westen D, Wirestam R, Stahlberg F, Latt J. A mechanism for exchange between intraaxonal and extracellular water: Permeable nodes of Ranvier. Proc ISMRM. 2010b: 1570.

Panagiotaki E, Schneider T, Siow B, Hall MG, Lythgoe MF, Alexander DC. Compartment models of the diffusion MR signal in brain white matter: a taxonomy and comparison. Neuroimage. 2012; 59:2241–54. [PubMed: 22001791]

Peled S. New perspectives on the sources of white matter DTI signal. IEEE Trans Med Imaging. 2007; 26:1448–55. [PubMed: 18041260]

Peled S, Cory DG, Raymond Sa, Kirschner Da, Jolesz Fa. Water diffusion, T2, and compartmentation in frog sciatic nerve. Magn Reson Med. 1999; 42:911–8. [PubMed: 10542350]

Qin W, Yu CS, Zhang F, Du XY, Jiang H, Yan YX, Li KC. Effects of echo time on diffusion quantification of brain white matter at 1.5T and 3.0T. Magn Reson Med. 2009; 61:755–60. [PubMed: 19191286]

Rose SE, Chen F, Chalk JB, Zelaya FO, Strugnell WE, Benson M, Semple J, Doddrell DM. Loss of connectivity in Alzheimer's disease: an evaluation of white matter tract integrity with colour coded MR diffusion tensor imaging. J Neurol Neurosurg Psychiatry. 2000; 69:528–30. [PubMed: 10990518]

Sen PN, Basser PJ. A model for diffusion in white matter in the brain. Biophys J. 2005; 89:2927–38. [PubMed: 16100258]

Stanisz GJ, Henkelman RM. Diffusional anisotropy of T2 components in bovine optic nerve. Magn Reson Med. 1998; 40:405–10. [PubMed: 9727943]

Stanisz GJ, Szafer A, Wright Ga, Henkelman RM. An analytical model of restricted diffusion in bovine optic nerve. Magn Reson Med. 1997; 37:103–11. [PubMed: 8978638]

Stejskal E, Tanner J. Spin Diffusion Measurements: Spin Echoes in the Presence of a Time-Dependent Field Gradient. J Chem Phys. 1965; 42:288.

Stewart, Wa; MacKay, aL; Whittall, KP.; Moore, GR.; Paty, DW. Spin-spin relaxation in experimental allergic encephalomyelitis. Analysis of CPMG data using a non-linear least squares method and linear inverse theory. Magn Reson Med. 1993; 29:767–75. [PubMed: 8350719]

Szafer, a; Zhong, J.; Gore, JC. Theoretical model for water diffusion in tissues. Magn Reson Med. 1995; 33:697–712. [PubMed: 7596275]

Tanner JE. Use of the Stimulated Echo in NMR Diffusion Studies. J Chem Phys. 1970; 52:2523–6.

Vasilescu V, Katona E, Simplaceanu V, Demco D. Water compartments in the myelinated nerve. III Pulsed NMR results. Experientia. 1978; 34:1443–4. [PubMed: 309823]

Vavasour IM, Whittall KP, MacKay aL, Li DK, Vorobeychik G, Paty DW. A comparison between magnetization transfer ratios and myelin water percentages in normals and multiple sclerosis patients. Magn Reson Med. 1998; 40:763–8. [PubMed: 9797161]

Vestergaard-Poulsen P, Hansen B, Ostergaard L, Jakobsen R. Microstructural changes in ischemic cortical gray matter predicted by a model of diffusion-weighted MRI. J Magn Reson Imaging. 2007; 26:529–40. [PubMed: 17685422]

Wachowicz K, Snyder RE. Assignment of the T2 components of amphibian peripheral nerve to their microanatomical compartments. Magn Reson Med. 2002; 47:239–45. [PubMed: 11810666]

Wang Y, Wang Q, Haldar JP, Yeh F-CC, Xie M, Sun P, Tu T-WW, Trinkaus K, Klein RS, Cross AH, Song S-KK. Quantification of increased cellularity during inflammatory demyelination. Brain. 2011; 134:3590–601. [PubMed: 22171354]

Zhang H, Schneider T, Wheeler-Kingshott Ca, Alexander DC. NODDI: Practical in vivo neurite orientation dispersion and density imaging of the human brain. Neuroimage. 2012; 61:1000–16. [PubMed: 22484410]

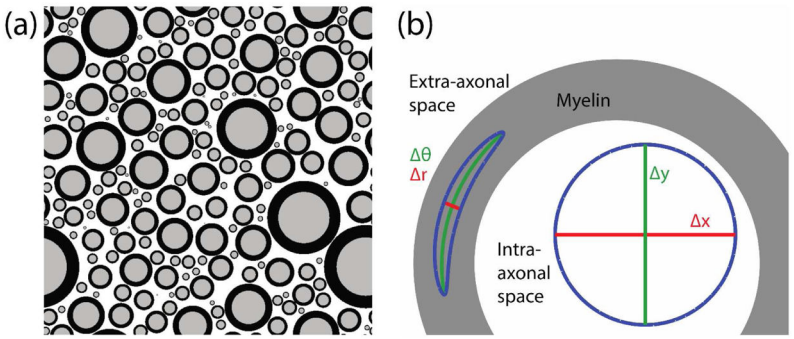


**Fig 1.**

(a) An example geometry showing a distribution of axon sizes with $\bar{R} = 1$ μm, $v_e = 0.35$, and $g = 0.7$. (b) Zoom in view of a myelinated axon, showing isotropic diffusion in intra- and extra-axonal space, as well as diffusion that is radially anisotropic within myelin.

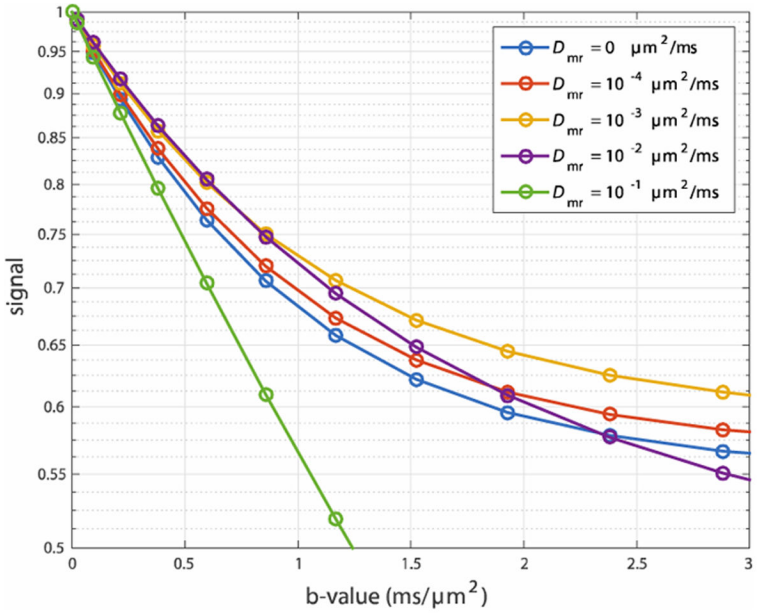


**Fig 2.**

The diffusion-weighted signal (log scale) vs b-value for a five values of the myelin water diffusion coefficient. The simulations used a geometry with $\bar{R} = 1$ μm, $v_i = 0.35$, and $g = 0.7$.

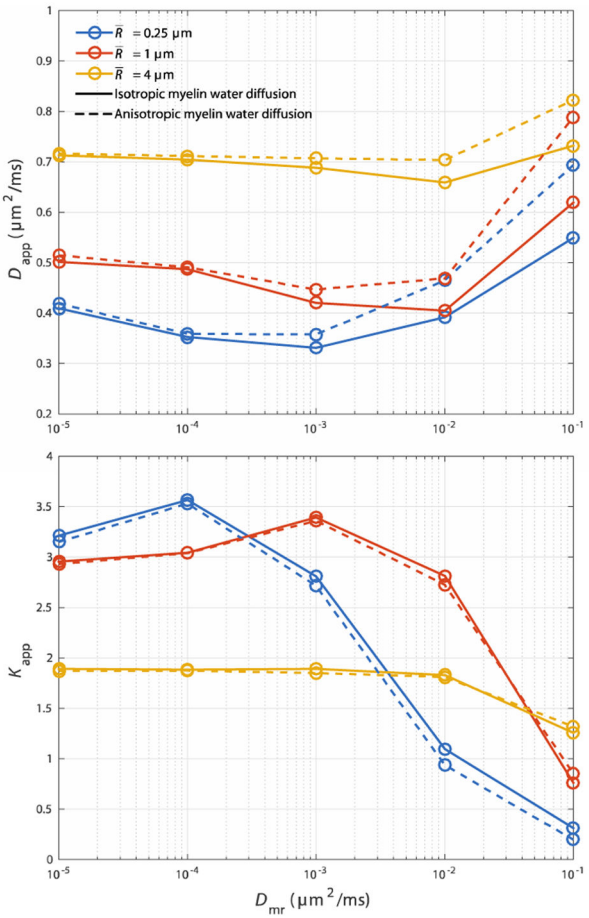


**Fig 3.**

The influence of the myelin water diffusion coefficient ($D_{mr}$) on $D_{app}$ and $K_{app}$ at $\bar{R}$ = 0.25, 1 & 4 μm, $g$ = 0.7 and $v_i$ = 0.35. Solid lines show values where myelin water diffusion is isotropic ($D_{mc}$ = $D_{mr}$), while dashed lines show values where myelin water diffusion is anisotropic ($D_{mc}$ = $D_0$).

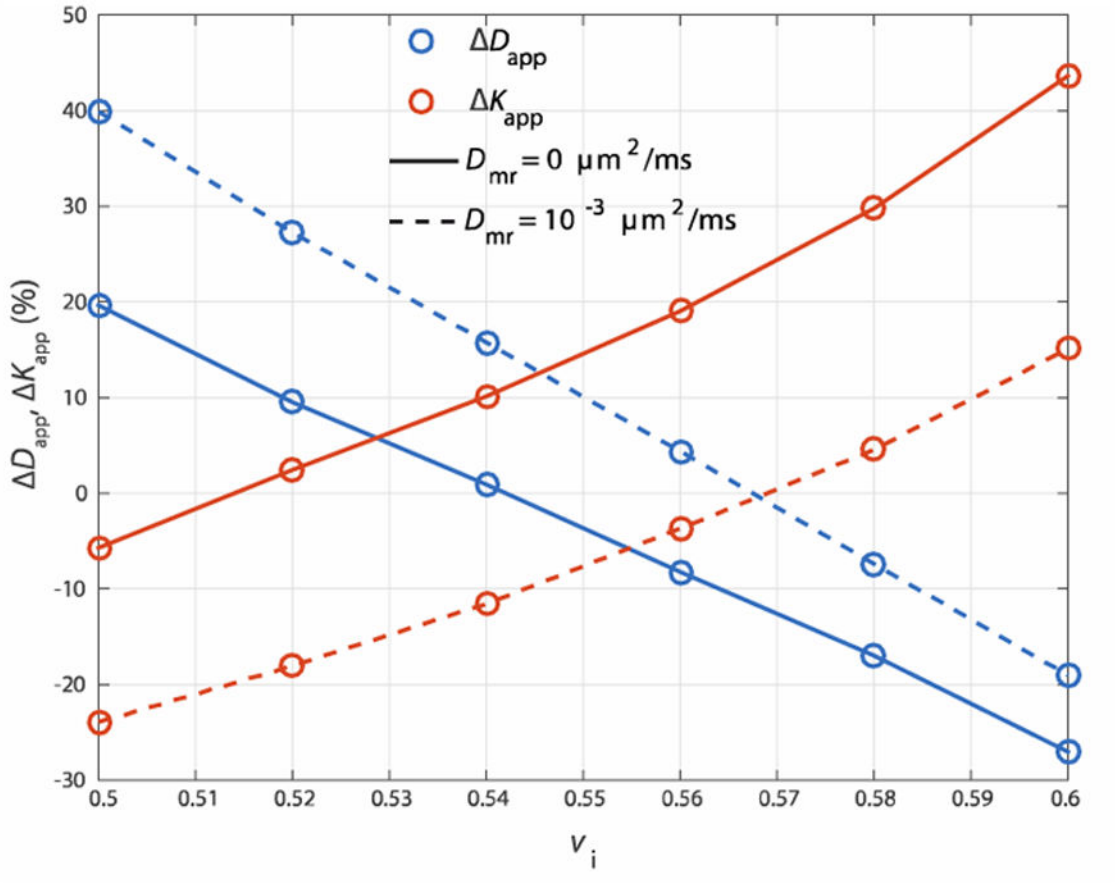


**Fig 4.**

Change in $D_{app}$ (blue) and $K_{app}$ (red) caused by a decrease in $v_m$ from 0.36 to 0.10, calculated over a range in relevant $v_i$ in the absence (solid lines) or presence (dashed line) of myelin water diffusion.

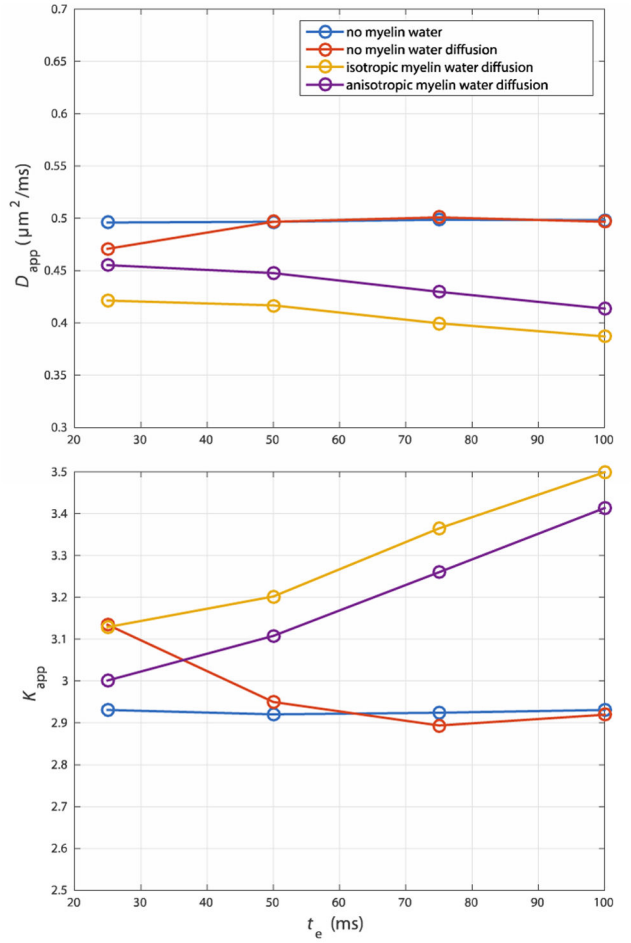


**Fig 5.**

When myelin water diffusion is neglected, $D_{app}$ decreases and $K_{app}$ increases with an increase in myelin water weighting (i.e. a decrease in TE) shown at $\bar{R} = 1$ μm, $v_i = 0.35$. However, modeling of myelin water diffusion reverses trends in $D_{app}$ and $K_{app}$ with TE.

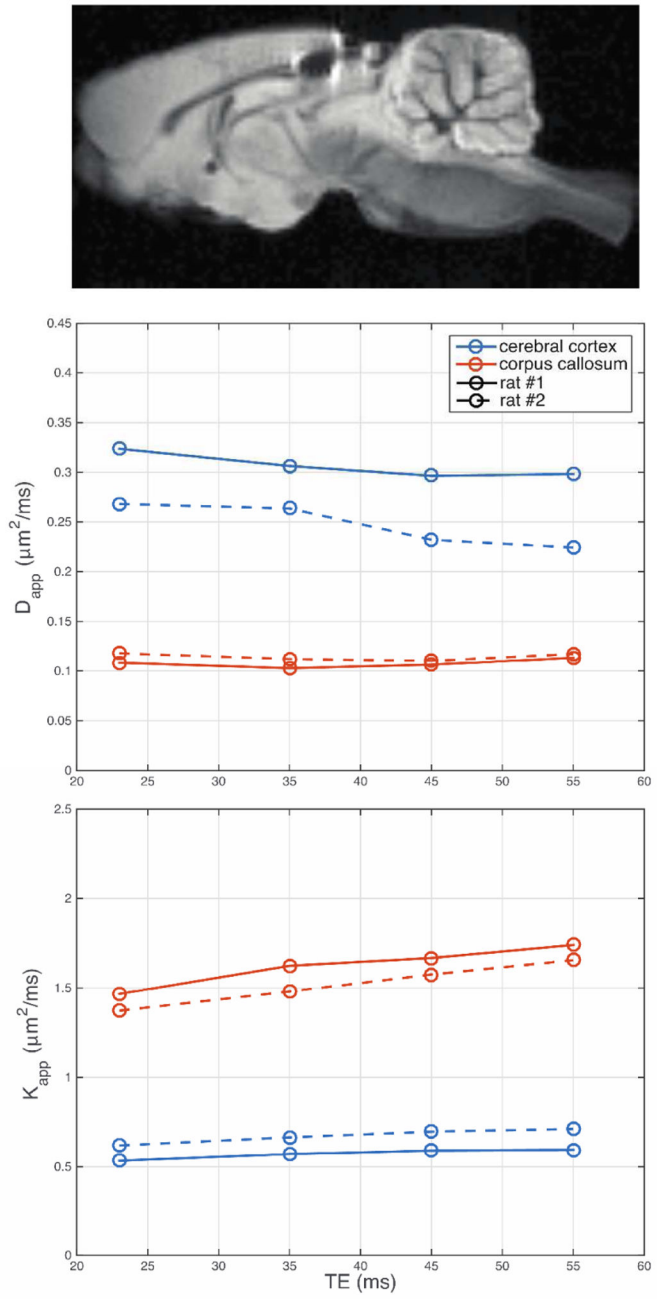


**Fig 6.**

$D_{app}$ and $K_{app}$ measured in the cerebral cortex and corpus callosum from two *ex vivo* rat brains.